ELSEVIER

Polymer 44 (2003) 719–727

polymer

www.elsevier.com/locate/polymer

Observation of melt fracture of polypropylene resins in capillary flow

Zhenghong Tao, Jan-Chan Huang*

Department of Plastics Engineering, University of Massachusetts Lowell, Lowell, MA 01854, USA

Received 29 August 2002; received in revised form 22 October 2002; accepted 25 October 2002

Abstract

Melt fracture, shear viscosity, extensional viscosity, and die swell of two polypropylene resins were studied using a capillary rheometer. A modified Bagley plot with consideration of pressure effects on melt viscosity and end effect was used. From the true wall shear stress the shear viscosity was calculated. Extensional viscosity was calculated from the end effect. Both shear and extensional viscosities of different molecular weights and temperatures correlated well under the time–temperature Williams–Landel–Ferry (WLF) superposition. Die swell increased when shear stress increased, and was higher for shorter dies at a given shear rate. When shear rates increased the extrudate staged from smooth to gross melt fracture with regular patterns (spurt), and then turned into irregular shapes. In the regular stage the wavelength of extrudates was measured, and corresponding frequency was calculated. The frequency increased when molecular weight decreased and when melt temperature increased. The shift factor based on shear viscosity also brought frequency data of different molecular weights and temperatures into master curves. The frequency decreased slightly when die lengths increased from $L/R = 10$ to 60. A small maximum was observed when shear rates increased.

Keywords: Melt viscosity; Melt fracture; Polypropylene

1. Introduction

Melt fracture is a flow instability phenomenon occurring when polymer melts are extruded through a die at rates exceeding a critical shear stress. Most of the previous studies on melt fracture of polymers focused on the behavior of various types of polyethylenes (HDPE, LDPE, and LLDPE) [1–26]. The melt fracture of PE is complicated. There are two types of melt fractures. At low shear rate, when the flow rate increases, the extrudate develops a small-amplitude high-frequency disturbance on its surface, which is called sharkskin. Sharkskin generally occurs at low shear rate for polymers with narrow molecular weight distribution. This is also known as surface melt fracture. The second type of melt fracture occurs at higher shear rates than sharkskin. It has different behaviors depending on the type of flow. In a system with controlled piston speed, a pressure oscillation can be observed and large amplitude quasi-periodic oscillation may appear on the extrudates. The flow is sometimes called a spurt flow. This is also called regular melt fracture in this paper. If the flow is a controlled pressure mode, a flow curve hysteresis occurs in some ranges of shear stress where two different flow rates are possible. This is accompanied by a discontinuity in the plot of flow rate versus pressure drop. High density polyethylene (HDPE) of high molecular weight tends to be free of sharkskin and enters directly into spurt stage when shear rate increases. For linear low density polyethylene (LLDPE) sharkskin is frequently encountered preceding the spurt.

Besides the difference in the shear rate at which melt fracture is observed, sharkskin and spurt also differ in their frequency. The frequency of spurt is on the order of 1 s^{-1} or lower, while sharkskin can have a frequency on the order of 100 s^{-1} [3,9,27]. Many studies were devoted to sharkskin and spurt phenomena of PE. Two types of theories were proposed for the mechanism of sharkskin. One is based on stick-slip at the die wall [2,3,13–15] and the other is based on the periodic growth and relaxation of tensile stress at the extrudate surface at the die exit [16–22,25,26]. The spurt phenomenon has been interpreted by the stick-slip phenomenon near the capillary surface [1–6], compressibility of polymer melts [7], combination of compressibility and slip [8,9,23,24], or constitutive instability of polymer melts [10–12].

The melt fracture of polypropylene (PP) was also studied

* Corresponding author.
E-mail address: jan_huang@uml.edu (J.C. Huang).

0032-3861/03/$ - see front matter © 2002 Elsevier Science Ltd. All rights reserved.
PII: S0032-3861(02)00830-3

in the literature. It is simpler than that of PE. A very important difference from PE was that no discontinuity in flow curve was observed. Ui et al. [27] reported continuous smooth curves without discontinuity for PP. At 180 °C the shape of the fractured extrudate surface obtained was fairly regular. They also noted that the wavelengths of the regular melt fracture increased as the shear rate increased, and that at higher shear rates perfectly smooth extrudates were obtained. When the shear rate was increased even more, a second sharp roughness appeared on the surface of the extrudate. The melt fracture occurred at a critical wall shear stress value in the range of 0.1–0.13 MPa, independent of temperature in the range 180–260 °C. Ballenger et al. [28] also reported that the extrudate shape changed from smooth to pitched screw threads, to smooth, and finally to a distorted form as shear rate increased. Bartos [29] studied the melt fracture behavior of a series of PPs to examine the critical conditions for the onset of extrudate distortions. He found that melt fracture occurred at a wall shear stress in the range of 0.069–0.16 MPa. Baik and Tzoganakis [30] studied the melt fracture of a series of PPs prepared by peroxide oxidation. The critical stress was found to decrease linearly from 0.15 to 0.10 MPa when the weight average molecular weight was increased from 100,000 to 400,000. Recently Fujiyama and Inata [31] observed sharkskin in narrow molecular weight PP-type thermoplastic elastomer and controlled-degradation PP at shear rate one order lower than those observed for spurt. They also proposed to use small amounts of adhesives such as maleated PP to promote adhesion and suppress sharkskin [32].

Most pervious studies on melt fracture of PP emphasized the critical shear stress at the inception of melt fracture. The observation of periods or frequency during melt fracture stages was rarely reported. Recently Wang et al. [23,24] measured the critical shear stress of a liner HDPE at different temperature under controlled pressure and found that the results of stress versus shear rate at different temperature could be superimposed by the WLF (Williams–Landel–Ferry) method. In later articles Wang et al. [25,26] also reported that the frequency of sharkskin of LLDPE at different temperatures could be superimposed by the WLF method. In our previous study [33] using Atofina 3181, a high molecular weight PP with 0.75 melt flow index (MFI), we have reported that the wavelength of extrudates in the regular melt fracture region increased when the shear rate was increased. However, the frequency of regular melt fracture was almost constant with respect to shear rates and decreased slightly when die length was increased. The purpose of this paper is to continue the study on the effect of molecular weight and temperature on melt fracture frequency and other relevant properties.

2. Experimental

The PP resins used in this study were Atofina 3181 and Atofina 3429 obtained from Atofina. Both PPs were a commercial grade homopolymer and contained additives to prevent oxidation and degradation during processing. The melt flow indices measured by ASTM D1238 condition L were 0.75 and 12 g/10 min, respectively. For Atofina 3181 the number average molecular weight (M_n) was 84,000 and the weight average molecular weight (M_w) was 512,000. For Atofina 3429 the number average molecular weight (M_n) was 40,000 and the weight average molecular weight (M_w) was 280,000. This information was provided by the company. A Galaxy V capillary rheometer (Kayness Inc., Model 8025) and tungsten carbide capillary dies with flat entrance region were used. The capillary is a constant extrusion speed type. Eighteen shear rates were used. The diameter was 0.10 cm and the lengths were 0.50, 2.0, and 3.0 cm. These gave length-to-radius (L/R) ratios of 10, 40, and 60, respectively. Temperatures of 190 and 220 °C were chosen for this study. A Brabender single screw extruder was used to mix the two PP resins to obtain a 50/50 weight blend. Temperature of extrusion was 220 °C.

3. Results and discussion

3.1. General observation of melt fracture

The melt fracture of PP was observed from extrudates. When melt fracture occurred the extrudate no longer maintained smooth cylindrical geometry. Fig. 1 shows the extrudates of Atofina 3429 collected at 190 °C from the shortest die. The results of Atofina 3181 were reported in a previous paper [33]. The melt fracture was more noticeable for the short die. The melt fracture became visible when apparent shear rates exceeded 800 s^{-1}. It was also observed that regular patterns appeared on extrudates between 800 and 2000 s^{-1}. At even higher shear rates the extrudate showed an irregular pattern. Within the shear rate ranges of this study there was no second smooth extrudate region. When melt fracture appeared as periodical pattern, the

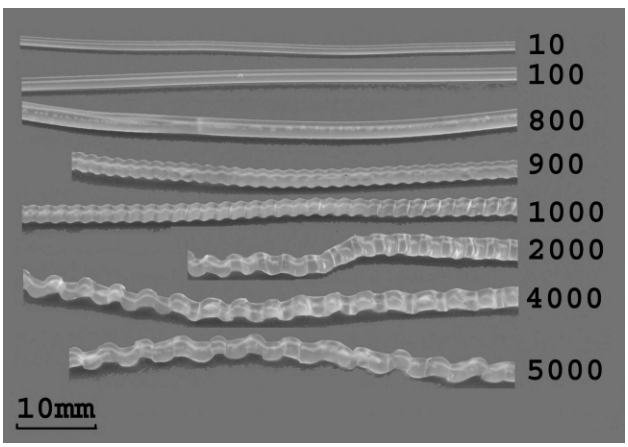

Fig. 1. Extrudates of Atofina 3429 at 190 °C and die length = 10 mm. Numbers indicate the apparent shear rates.

wavelength of extrudates was measured. It was noted that when shear rate was increased, the wavelength increased. As die length was increased, the start of a regular pattern was delayed to a higher shear rate. A decrease in molecular weight of PP also delayed the start of regular melt fracture. The pattern of regular melt fracture appeared to be different from those reported by Baik and Tzogankis [30], but more similar to those reported by Kazatchkov et al. [34]. In the study of Baik and Tzogankis regular helix-like extrudates were observed at shear rate between 700 and 5000 s^{-1}; a smooth extrudate was observed between 6000 and 10,000 s^{-1}. At 20,000 s^{-1} and higher irregular extrudates were observed. In our study the shear rate range for regular melt fracture was narrower, and more complicated extrudates were obtained between shear rates of 800 and 2000 s^{-1}. The regular melt fracture in the study of Kazatchkov et al. appeared even earlier around 200 s^{-1} and turned into irregular at about 500 s^{-1}. The pattern of melt fracture of Kazatchkov et al. at 278 s^{-1} was similar to our results at 900 s^{-1}. In both conditions the shear stresses were about 0.12 MPa. The PP used by Baik and Tzogankis [30] had M_w of 231,000 and $M_w/M_n = 7.65$. The M_w of Atofina 3429 was 280,000 and the M_w/M_n was 7.0. The molecular weight of PP used by Kazatchkov et al. was much higher with $M_w = 762{,}000$ and $M_w/M_n = 10.0$. The difference in extrudate patterns could be a result of higher elastic energy due to higher molecular weight.

3.2. Apparent flow curve

Fig. 2 shows the apparent shear stress, $\tau_a = R\Delta P/2L$, versus the apparent shear rate, $\dot{\gamma}_a = 4Q/\pi R^3$ (Q is volume flow rate), of PP 3429 at 190 °C for the three dies. This plot was commonly used to identify the existence of melt fracture and wall slip [1–4]. For PE, polybutadiene, and polyisoprene the melt fracture was accompanied with a discontinuity in the shear stress versus shear rate curve [5]. No such phenomenon was seen in this study. Kazatchkov et al. [34] and Ui et al. [27] reported breaks in the plot of apparent shear stress versus apparent shear rate. No clear break could be seen in Fig. 2 but a divergence of data was seen at apparent shear rates above 100 s^{-1}. The trend of curves continued into the melt fracture region. Since PP 3429 had low molecular weight, the melt fracture occurred only at apparent shear rates above 800 s^{-1}. At 2000 s^{-1} the melt fracture turned into irregular.

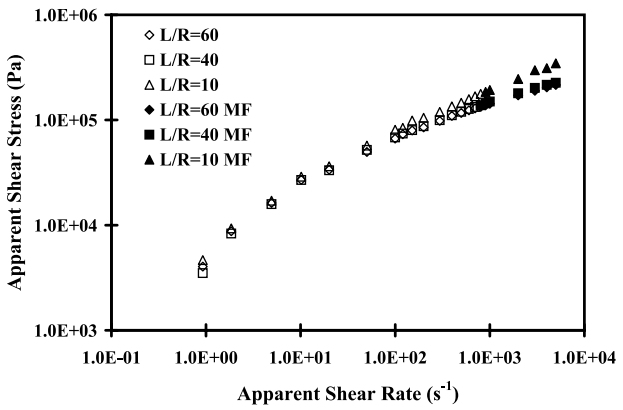

Fig. 2. Apparent shear stress versus apparent shear rate of Atofina 3429 at 190 °C for three die lengths. Filled symbols indicate melt fracture.

3.3. End effect and pressure effect on viscosities

The apparent shear stress increased when apparent shear rate was increased in Fig. 2, but at the high shear rate region the slope was lower than at the low shear rate region. This is typical for a material exhibiting a shear thinning phenomenon. The curves of the two longer dies overlapped each other and had lower shear stress than the shortest die in the high shear rate region. When pressure drop of each flow rate was plotted versus L/R, an upward trend was observed as in our previous studies [33,35]. This was explained by the pressure dependence of shear and extensional viscosities. The following function has been used to describe the effect of pressure on shear viscosity [33–40]

$$\eta = \eta_0 \, e^{\beta P} \tag{1}$$

where η_0 is the shear viscosity at zero pressure and β is the pressure coefficient. A similar expression has also been used to describe the pressure dependency on extensional viscosity [33,35,40,41]

$$\eta_e = \eta_{e,0} \, e^{\alpha P} \tag{2}$$

where $\eta_{e,0}$ is the extensional viscosity at zero pressure and α is the pressure coefficient.

When there is no pressure effects on viscosity, the plot of pressure drop versus die length is a straight line. This is the well-known Bagley plot [42]:

$$\Delta P = 2\tau_{tw}(L/R + e) \tag{3}$$

Here the dimensionless e is the end effect. It is generally considered to be constant when dies with different lengths are measured at the same shear rate. When the pressure dependency on shear viscosity was considered integration of pressure from die entrance to exit gave [37–39]:

$$[1 - \exp(-\beta\Delta P)]/\beta = 2\tau_{tw}(L/R + e) \tag{4}$$

The end effect could also be affected by the high pressure in the barrel of capillary rheometer. The relationship between the end effect and extensional viscosity, η_e, and shear viscosity was derived by Cogswell [43]. In his analysis, it was assumed that the polymer melt adopts a coni-cylindrical flow pattern as it passes from the reservoir into the capillary, and that this pattern corresponds to minimum entrance pressure drop. Also, it was assumed that the shear viscosity of the polymer melt could be described in terms of a power-law model. Following this analysis, the extensional viscosity, η_e, and the extensional strain rate, $\dot{\epsilon}$, were calculated

as:

$$\eta_e(\dot{\epsilon}) = \frac{9}{32}\frac{(n+1)^2\Delta P_e^2}{\eta(\dot{\gamma}_a)\dot{\gamma}_a^2} \quad (5)$$

$$\dot{\epsilon} = \frac{4}{3}\frac{\eta(\dot{\gamma}_a)\dot{\gamma}_a^2}{(n+1)\Delta P_e} \quad (6)$$

where $\dot{\gamma}_a$ is the apparent shear rate, n (= d log τ_a/d log $\dot{\gamma}_a$) is the power law exponent, ΔP_e is the entrance pressure drop corresponding to zero capillary die length, and $\eta(\dot{\gamma}_a)$ is the shear viscosity. Using the relation between entrance pressure drop and end effect, $\Delta P_e = 2e\tau_{tw} = 2e\eta(\dot{\gamma}_a)\dot{\gamma}_a$, Eq. (5) can be changed to:

$$e = \frac{2\sqrt{2}}{3(1+n)}\sqrt{\eta_e(\dot{\epsilon})/\eta(\dot{\gamma})} \quad (7)$$

With the consideration of pressure effect on shear viscosity and extensional viscosity, the end effect can be separated into a product of the zero pressure component E and its pressure dependency. The dependence of the end effect on pressure is: $e = E\exp[(\alpha-\beta)\Delta P/2]$. Using this new form of end effect and Eq. (4) the following equation can be derived [33]:

$$[1-\exp(-\beta\Delta P)]\exp[-(\alpha-\beta)\Delta P/2]/\beta = 2\tau_{tw}\{(L/R)\exp[-(\alpha-\beta)\Delta P/2]+E\} \quad (8)$$

Here τ_{tw} is the true wall shear stress and E is the end effect, both at zero pressure. The ΔP is the barrel pressure where the end effect took place. When values of α and β are small Eq. (8) reduces to the Bagley equation. If parameters α and β are known the left-hand side of Eq. (8) can yield a linear plot versus $(L/R)\exp[-(\alpha-\beta)\Delta P/2]$.

Recently, Binding et al. [40] determined the pressure dependency of shear viscosity and extensional viscosity of several polymers using a capillary rheometer that could be pressurized at both entrance and outlet. The values of α and β obtained by Binding et al. [40] were used in this study. The values of α and β at 190 °C were 19.1 and 7.1 GPa^{-1}, respectively. The values at 220 °C were 16.4 and 6.8 GPa^{-1}, respectively. Fig. 3 shows the left hand side of Eq. (8) versus $(L/R)\exp[-(\alpha-\beta)\Delta P/2]$ for selected apparent shear rates of PP 3429 at 190 °C. Good linear lines are seen in Fig. 3. From a linear regression calculation, the values of τ_{tw} and E were determined.

The end effect at zero pressure E was plotted versus the true wall shear stress in Fig. 4. The result of end effect showed that there were two transitions, separating data into three zones. One transition occurred near 0.08 MPa and the other at 0.13 MPa. At the stress below the first critical stress the end effect increased slowly when stress increased. Between the first and the second critical shear stresses, the end effect increased at a higher rate. During this stage the trend of end effect of Atofina 3429 was very similar to that of Atofina 3362 [35] and Atofina 3181 [33] reported earlier. Several authors have studied the critical stress of melt

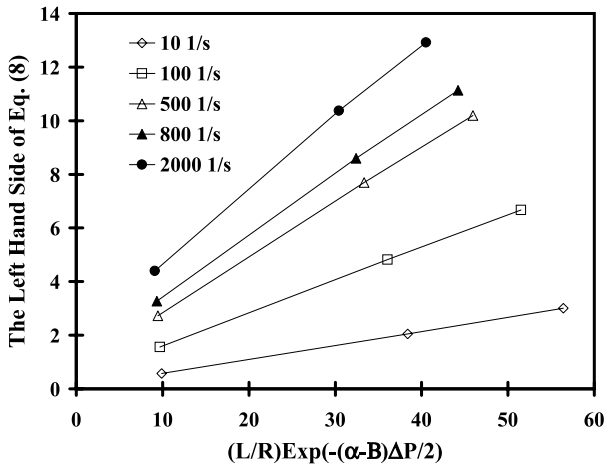

Fig. 3. The left hand side of Eq. (8) versus $(L/R)\exp(-(\alpha-\beta)\Delta P/2)$ for selected apparent shear rates of PP 3429 at 190 °C. Filled symbols indicate melt fracture.

fracture of PP based on the observation of extrudates [27–35]. In particular, Baik and Tzoganakis [30] studied the melt fracture of a series of PPs prepared by peroxide oxidation. They reported that the critical stress decreased linearly from 0.15 to 0.10 MPa when the weight average molecular weight was increased from 100,000 to 400,000. The M_w of Atofina 3429 was 280,000 and the regular melt fracture in this study started at 0.12 MPa. This agreed with the above range. It is noted that the increase in the end effect was not significant until the onset of irregular melt fracture. This indicated that in the regular melt fracture stage the energy loss was not significantly increased yet. In the irregular stage of melt fracture the energy loss increases much more quickly and is manifested as a sharp increase of the end effect, as well as die swell which will be discussed later. The transition from zone one to zone two could be assigned as the start of regular melt fracture, while the second critical shear stress corresponded to the transition to irregular melt fracture. However, the observation of regular

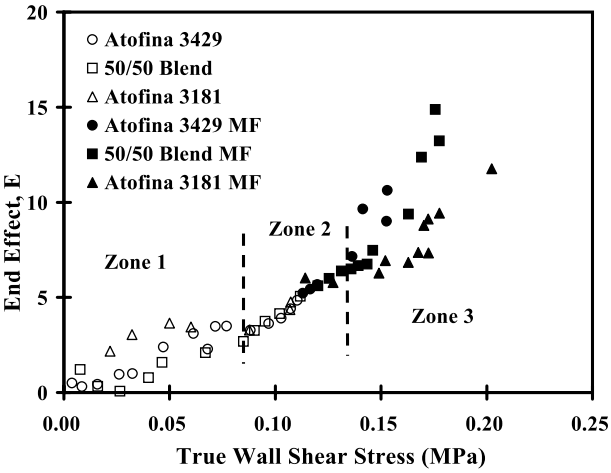

Fig. 4. End effect at zero pressure versus true wall shear stress of Atofina 3181, Atofina 3429 and 50/50 blend at 190 °C. Filled symbols indicate melt fracture.

Table 1
The shift factor of polypropylene relative to PP 3181 at 190 °C

Materials	Shift factor, a_T
PP 3429 at 190 °C	0.24
50/50 blend at 190 °C	0.61
PP 3181 at 220 °C	0.56

melt fracture did not coincide with the transitions in Fig. 4. The melt fracture regions were shown as filled symbols, which started in the middle of zone two but a large increase in the end effect occurred in zone three. In a previous study [38] of our laboratory we have also reported that for a metallecene copolymer of ethylene and octene the observation of melt fracture preceded the large increase of the end effect. In view of these results the determination of critical shear stresses for the transition between the smooth stage and regular/irregular melt fracture should also be compared with the end effect measurement.

3.4. True shear viscosity

The calculation of shear viscosity started from a plot of the true wall shear stress, τ_{tw}, versus the apparent shear rate, $\dot{\gamma}_a$, on a double logarithm scale. The slope n of this plot was used to make the Rabinowitsch correction. The Rabinowitsch correction was made to calculate the true shear rate on capillary surface, $\dot{\gamma}_{tw}$, from the apparent shear rate, $\dot{\gamma}_a$:

$$\dot{\gamma}_{tw} = \dot{\gamma}_a(3n+1)/4n \tag{9}$$

The shear viscosity is calculated as:

$$\eta = \tau_{tw}/\dot{\gamma}_{tw} \tag{10}$$

Melt viscosity results of polymers with different molecular weights can be superimposed with proper adjustment of parameters. A superposition of data can be made for shear viscosity based on the following formula [44]:

$$\eta(T)T_0/a_T T_R = f(a_T\dot{\gamma}) \tag{11}$$

where a_T is the WFL shift factor and the subscript R indicates the reference molecular weight or temperature. The results were listed in Table 1. For polymers with different molecular weights measured at the same temperature, the shift factor represents the ratio of Newtonian viscosity. For the same polymer measured at different temperatures the shift factor is related to flow activation temperature of melts. Eq. (11) predicts a master shear viscosity curve which is shown in Fig. 5. It can be seen that the shear viscosities of Atofina 3181, Atofina 3429 and the 50/50 blend overlapped well after the shifting. This indicated that both polymers had similar rheological behaviors. The results of shear viscosity in Fig. 5 also showed a strong shear rate dependency in the shear rate region studied, which justified the use of the Rabinowitsch correction. At the low end of shear rates the melt viscosity had not reached the Newtonian region. At the high shear rate the power law exponent was estimated to be 0.23. It was noted that despite the occurrence of melt fracture, the viscosity results still showed a continuous trend. This indicated that in melt fracture stages, the increase of pressure drop due to melt fracture was zero or constant and was included in the end effect term in the linear plot of Eq. (8). This also suggested that the energy loss in melt fracture of PP was independent of die length and was likely to be associated with the entrance effect or was created at the die exit similar to the sharkskin of PE [16–24,45].

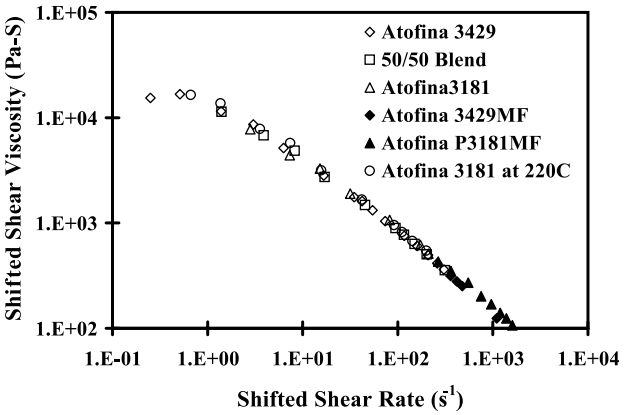

Fig. 5. Shifted shear viscosity ($\eta T_0/a_T T$) versus shifted shear rate ($a_T\dot{\gamma}$) of Atofina 3181, Atofina 3429, 50/50 blend at 190 °C, and Atofina 3181 at 220 °C using Atofina 3181 at 190 °C as the reference. Filled symbols indicate melt fracture.

For most unfilled polymers the shear viscosity at different temperature can be shifted into a master curve using a reference temperature. Fig. 5 included melt viscosity of Atofina 3181 at 220 °C shifted to 190 °C. The shift factor was 0.56. From the shift factor, the activation energy of shear viscosity was estimated to be 37 kJ/mol, which was less than the value of 46 kJ/mol obtained for a different grade of PP, Atofina 3362, reported previously [35]. The error in calculating activation energy can be estimated from Arrhenius equation. A difference of 5% in the shift factor will result in error of 3 kJ/mol in activation energy and an 1 °C error in temperature will result in 1.1 kJ/mol in error. A difference in activation energy in PP with different molecular weight was also reported by Brandao et al. [46]. In their study the activation energy of a PP with higher molecular weight was less than that of a low molecular weight grade.

3.5. Extensional viscosity

The extensional viscosity results of Atofina 3429, Atofina 3181, and the 50/50 blend are shown in Fig. 6. A WLF shift, using the shift factor obtained from shear viscosity, was made to compare extensional viscosity of PP with different molecular weights. It can be seen that, after the shift, results of both PPs and the blend overlapped very well. Extensional viscosity of a series of PPs was measured

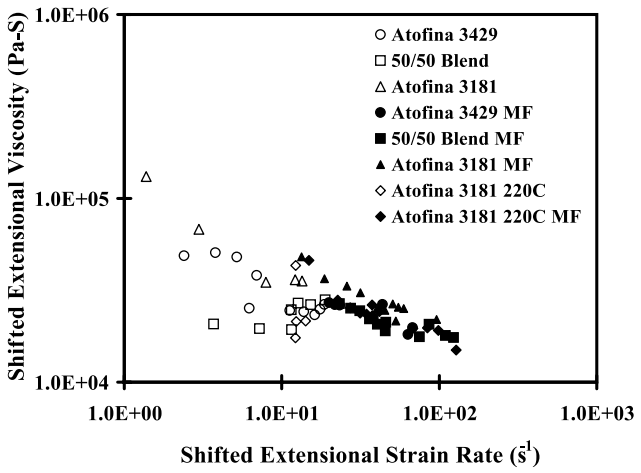

Fig. 6. Shifted extensional viscosity ($\eta_e T_0/a_T T$) versus shifted extensional strain rate ($a_T\dot{\epsilon}$) of Atofina 3181, Atofina 3429, 50/50 blend at 190 °C, and Atofina 3181 at 220 °C using Atofina 3181 at 190 °C as the reference. Filled symbols indicate melt fracture.

by Tzoganakis et al. [47] from end effects using Eqs. (5) and (6). The extensional viscosity of a sample with $M_w = 267{,}300$ was about 6000 Pa s at 100 s^{-1}. Our result of Atofina 3429 before the shift was 6200 Pa s, which agreed well. At low strain rate, extensional viscosity decreased as a power law function when strain rate was increased. At the strain rate corresponding to the regular and irregular melt fracture regions, the slope decreased. This deviation from the trend originated from the high values of the end effect above the critical shear stresses. A high value of the end effect could be attributed to the melt fracture phenomenon, which formed another source of pressure drop and end effect. A comparison of Eqs. (5) and (6) shows that an additional increase in ΔP_e increases η_e twice as fast as it decreases $\dot{\epsilon}$ in a double log plot. Therefore, in Fig. 6 the data in melt fracture regions deviated upward and had a slope near -0.5.

3.6. Die swell

Die swell data of Atofina 3429 at 190 °C is reported in Fig. 7 and a comparison of three PPs at 190 °C with die of $L/R = 60$ is made in Fig. 8. The die swell ratio was measured as the ratio of the solid extrudate diameter (D_{ex}) to the diameter of the die (D). When melt fracture occurred, die swell increased and the diameter became irregular. Therefore, the average diameter was calculated based on measurement of mass of extrudates using 8 cm length of extrudates. The results on Atofina 3181 were reported earlier [33]. Fig. 7 showed that, when die length was increased, die swell decreased. This was because some of strain created at the die inlet was relaxed after sufficient die length. It can also be seen that die swell increased continuously after the onset of regular melt fracture. A small change in slope was observed at 1.2×10^5 Pa, which was similar to the critical shear stress of melt fracture determined by extrudate observation. Fig. 8 compares the die swell of the three PPs in the longest die. It is noted that in melt fracture stage the die swell of the 50/50 blend was higher than both Atofina 3181 and Atofina 3429. When die swell was plotted versus apparent shear rate, the curves of Atofina 3181 and 50/50 blend were very close, with the latter being slightly smaller. The relatively high curve for die swell of 50/50 blend might result from a wider molecular weight distribution for the 50/50 blend. Compared to the parent polymers. In a study by Vlachopoulos et al. [48] it was concluded that molecular weight distribution had a large influence on die swell for polystyrene.

3.7. Frequency of melt fracture

For polyethylene, surface melt fracture (sharkskin) usually occurs before gross melt fracture [1–8]. However, this type of distortion did not occur in the case of PP [27–30]. Only recently Fujiyama et al. [31] reported sharkskin in PP with narrow molecular weight distribution. After the critical stress the melt fracture of PP occurred as large amplitude periodical patterns. The wavelength increased when shear rate was increased as shown in Fig. 1. Since observed wavelength changed when extrudate was stretched, it is better to express the oscillation using frequency. The ratio between the average melt flow velocity at capillary exit and wavelength represents the frequency of oscillation. The frequency was calculated using the following formula:

$$\nu = \langle V\rangle/\lambda = \dot{\gamma}_a/D/8/\text{wavelength of solid} \times \text{extrudates}/(D_{ex}/D)^2/(\rho_{25C}/\rho_T) \quad (12)$$

where $\langle V\rangle$ is the average velocity at the die exit, λ is the wavelength measured at the die exit, D_{ex} is the diameter of the solid extrudate, and D is the diameter of the die. In Eq. (12) the measured wavelength of extrudates was adjusted by die swell and density ratio, ρ_{25C}/ρ_T, to reflect the actual wavelength at the die exit. Density values of a PP at room temperature and melt temperatures from Zoller and Walsh [49] were used. A similar equation was used by Wang et al. [26] in the calculation of periods of melt fracture in the sharkskin stage of LLDPE. The use of frequency avoids the dependency of extrudate wavelength on the gravitational sagging, because gravitational sagging increases wavelength and reduces extrudate diameter at the same time; the effect of both will be cancelled in the calculation. Fig. 9 shows the frequency of regular melt fracture versus the apparent shear rate for the long die and short die. The frequency of the long die was almost independent of the shear rate. For the short die, the frequency of Atofina 3429 showed an increasing trend when shear rate increased. Small maximum was seen in Atofina 3181 and the 50/50 blend. The onset of regular melt fracture was slightly delayed when high L/R die was used.

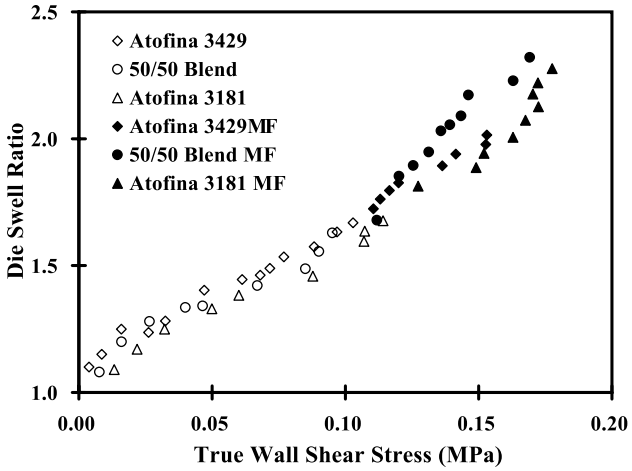

Fig. 7. Die swell ratio of Atofina 3429 at 190 °C for three dies. Filled symbols indicate melt fracture.

This agreed with the observation of Baik and Tzoganakis [30]. High *L/R* also decreased the shear rate for the transition to irregular melt fracture. In other words the shear rate range of regular melt fracture narrowed when die length was increased. From these observations regular melt fracture seemed to be related to the strain in capillary dies, which relaxed to a constant value for a long die. The surface melt fracture of PE was known to be dependent on the barrel size [3,9,50]. To observe any barrel size dependency we conducted extrusion studies of Atofina 3181 using full loaded barrel and programming from high shear rate to low shear rate and compared the results from low shear rate to high shear rate. It was found that the frequency was the same and independent of barrel size [33].

In Fig. 9 it can be seen that a decrease in molecular weight or increase in temperature increased frequency at a given shear rate. Since different PPs had similar critical shear stress, the factors determining the frequency of melt fracture appeared to be different from those determining the onset of melt fracture. Different frequency may be attributed

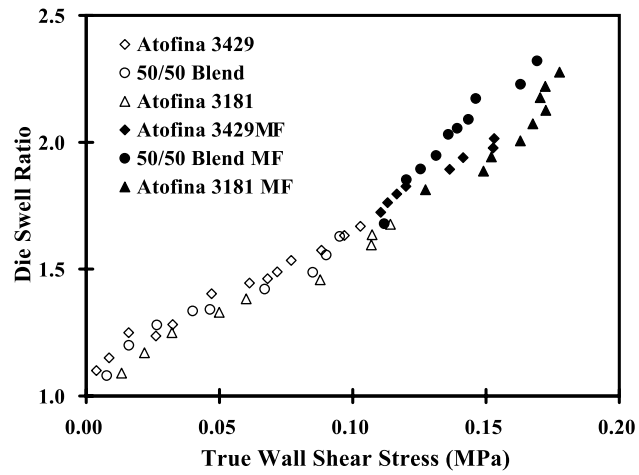

Fig. 8. Die swell ratio of Atofina 3181, Atofina 3429, and 50/50 blend at 190 °C of Die with $L/R = 60$. Filled symbols indicate melt fracture.

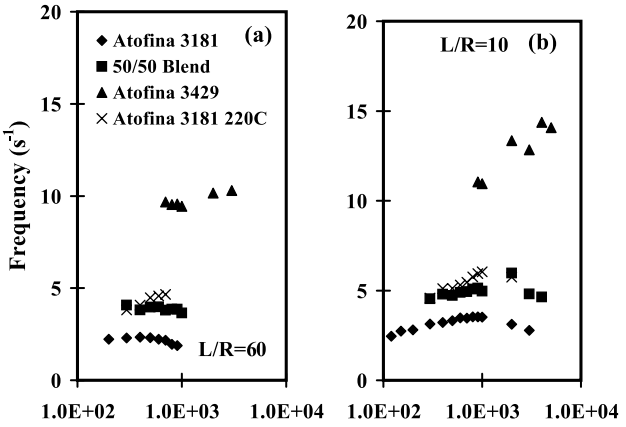

Fig. 9. Frequency of regular melt fracture versus apparent shear rate of Atofina 3181, Atofina 3429, 50/50 blend at 190 °C, and Atofina 3181 at 220 °C.

to change in melt viscosity or relaxation time associated with viscosity. If melt fracture frequency is related to melt viscosity, it can be shifted; and results of different samples can be superimposed together. Since both shear rate and frequency have the same dimension, 1/time, they will be shifted by the same factor. In Fig. 10 both frequency and shear rate were multiplied by the shift factor in Table 1. It can be seen that results formed master curves with the long die being slightly lower. The results of the medium die, which were not reported here, lay between two curves. A small maximum was also observed. The shear rate of the maximum increased slightly when the die length was decreased. The range of frequency was between 2 and 4 s^{-1}, which indicated that melt fracture of PP was similar to spurt phenomena of PE and not a high frequency sharkskin.

The mechanism commonly used to explain the spurt of PE is a slip-stick phenomenon combined with compressibility of melts. In this mechanism [51], high strain is first built up in melt in the area near the die surface, because shear stress is highest in that region. The polymer molecules are stretched in the flow direction and a slip occurs after the stress exceeds a threshold stress. During this stage a change

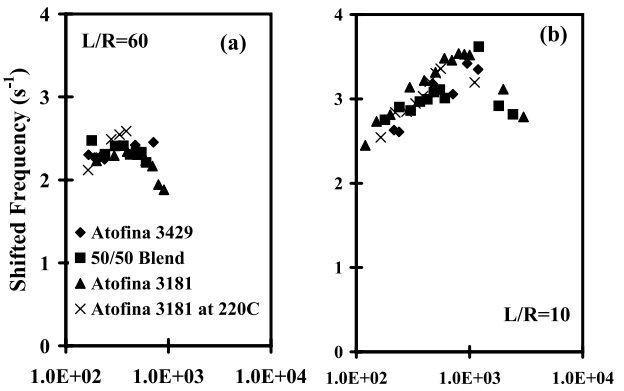

Fig. 10. Shifted frequency ($a_T \nu$) versus shifted apparent shear rate ($a_T \dot{\gamma}_a$) of Atofina 3181, Atofina 3429, 50/50 blend at 190 °C, and Atofina 3181 at 220 °C using Atofina 3181 at 190 °C as the reference.

in pressure or flow rate can be observed. After the slip the molecules relax and later the strain builds up and the process starts again. PP may involve similar processes. The fact that frequency can be superimposed together is a strong support that spurt phenomena of PP involves a strain-relaxation process. Our observation on the decrease of frequency with increasing die length is also in line with the above mechanism, because the strain would be higher for a shorter die where strain was just starting to relax from the die inlet. Another explanation is that a longer die would have a higher hydrostatic pressure and the relaxation process would be reduced because of higher viscosity. This led to a smaller frequency. The weak maximum observed in Fig. 10 can also be explained within the similar framework. In a recent work by Wang et al. [26] the Maxwell model was used to give a quantitative explanation on the mechanism for sharkskin. In the model the stress at wall is repeating a stress build up and decay process. During the decaying process the following equation was derived:

$$\sigma(t) = \sigma_s + (\sigma_c - \sigma_s)\exp(-t/\tau'), \qquad \text{for } 0 \le t < \tau_R \quad (13)$$

where σ_s is the stress corresponding to the shear rate at slip of wall, σ_c is the wall shear tress without slip, and τ' is the relaxation time of the Maxwell model. At the end of relax period, $t = \tau_R$, and the stress relaxed to $\sigma(\tau_R) = \sigma_h$. During the stress building process the following equation applied:

$$\sigma(t) = \sigma_h + \sigma_c\{1 - \exp[-t - \tau_R)/\tau']\}, \quad \text{for } \tau_R \le t < \tau_R + \tau_G \quad (14)$$

The overall oscillation period is given by:

$$\tau = \tau_R + \tau_G = \tau' \ln\left(\frac{R^2(S-1)}{(S-R)}\right) \quad (15)$$

where $R = \sigma_c/\sigma_h$ and $S = \sigma_c/\sigma_s$. The overall oscillation period is related to the time constant of the Maxwell model by a logarithmic factor. The value of R represents the ratio of upper bound, σ_c, and lower bound, σ_h, of stress during the oscillation. The values of σ_h and σ_c increased when extrusion rate increased but their ratio likely remained relatively constant at a value slightly higher than unity [52]. The value of S represents the ratio between the nominal (no slip) stress to the threshold stress, σ_s. The value of S is higher than R and increases when extrusion rate increases. If one keeps R constant and increases S the value of the log term decreases gradually. This could explain a gradual decrease of oscillation period and the increase of frequency when extrusion rate increased. A maximum of frequency cannot be predicted from Eq. (15) by changing R or S. We speculate two possibilities for the explanation. One is that the decrease in frequency at higher shear rate occurs because the linear Maxwell model no longer follows and the overall oscillation period becomes longer and the frequency decreases. The other possibility is that at higher shear rate the high pressure increases viscosity and decreases the time constant τ'. This is similar to one of the previous mechanisms to explain higher frequency of short die in Fig. 10. This argument is also supported by the fact the maximum of short die occurred at higher shear rate than the long die in Fig. 10. It would take a higher shear rate for the short die to reach the same pressure compared to the long die. The pressure effect argument would preclude the mechanism that spurt phenomena of PP is formed at die exit because at exit the pressure is small. It can be formed at die inlet or inside capillary wall.

Despite the similarity between spurt of PP and PE there are three major differences between spurt phenomena of PP and PE: (1) there is no flow discontinuity observed for neat PP yet, despite some reports about die slip measurement using dies with different diameter [31,34]. Akay reported flow discontinuity of short glass filled PP at temperatures of 270 and 300 °C at shear rates above 5×10^5 s^{-1} [53]. We felt that a different mechanism was involved in filled systems. (2) We have observed that there was no barrel volume dependency on spurt frequency in PP [33]. The volume dependency of frequency was reported in melt fracture of PE [3,9,50], which added support to the mechanism of melt fracture based on stick-slip and melt compressibility. (3) The frequency range of PP we measured was around 2–20 s^{-1}. The range lay between sharkskin and spurt of PE. Sharkskin generally has a frequency around 100 s^{-1} while frequency of pressure oscillation of spurt ranged from 0.05 to 1 s^{-1}. These are clues that spurt of PP may be different from PE. More work would be needed to explore the difference in melt fracture between PE and PP.

4. Conclusions

Melt fractures of two PPs and their 50/50 blend were observed in a capillary rheometer. The flow curve and extrudate appearance could be divided into three regions. In the low flow rate, smooth extrudate was obtained. At the next stage, melt fracture with regular patterns was observed. An equation including pressure effect on shear viscosity and extensional viscosity was used to calculate wall shear stress and end effect. Shear viscosity and extensional viscosity were calculated and correlated well under WLF superposition. The frequencies of regular melt fracture of the three compositions were also shifted by the same shift factors from melt viscosity. The master curves were nearly constant but showed a small maximum when shear rate was increased. The frequency was slightly higher for the short die.

Acknowledgements

The authors would like to express their special thanks to Dr R.D. Deanin of the Department of Plastics Engineering

at the University of Massachusetts Lowell for his invaluable help and useful discussion.

References

[1] Sornberger G, Quantin JC, Fajolle R, Vergnes B, Agasant JF. J Non-Newtonian Fluid Mech 1987;23:123–35.
[2] Ramamurthy AV. J Rheol 1986;30:337–57.
[3] Kalika DS, Denn MM. J Rheol 1987;31:815–34.
[4] Larson RG. Rheol Acta 1992;31:213–63.
[5] Denn MM. Ann Rev Fluid Mech 1990;22:13–34.
[6] Shore JD, Ronis D, Piche L, Grant M. Phys Rev Lett 1996;77:655–8.
[7] Weill A. Rheol Acta 1980;19:623–32.
[8] Hatzikiriakos SG. Polym Engng Sci 1994;34:1441–9.
[9] Hatzikirakos SG, Dealy JM. J Rheol 1992;36(5):845–84.
[10] McLeish TCB, Ball RC. J Polym Sci, Polym Phys Ed 1986;24: 1735–45.
[11] Lin YH. J Rheol 1985;29:605–37.
[12] McLeish TCB. J Polym Sci 1986;B25:2253–64.
[13] Kissi NE, Piau JM. J Non-Newtonian Fluid Mech 1990;37:55–94.
[14] Hatzikiriakos SG, Hong P, Ho W, Stewart CW. J Appl Polym Sci 1996;55:595–603.
[15] Ghanta VG, Riise BL, Denn MM. J Rheol 1999;43:435–42.
[16] Cogswell FN. J Non-Newtonian Fluid Mech 1977;2:37–47.
[17] Piau JM, Kissi NE, Tremblay BJ. J Non-Newtonian Fluid Mech 1990; 34:145–80.
[18] Moynihan RH, Baird DG, Ramanathan R. J Non-Newtonian Fluid Mech 1990;36:255–63.
[19] Tremblay BJ. J Rheol 1991;35:985–9.
[20] Kissi NE, Piau JM. J Rheol 1994;38:1447–63.
[21] Baird DG, Tong PP. SPE Technical Paper. 53 rd ANTEC; 1995. p. 1095–100.
[22] Kissi NE, Piau JM, Toussaint F. J Non-Newtonian Fluid Mech 1997; 68:271–90.
[23] Wang SQ, Drda PA. Macromolecules 1996;29:2627–32.
[24] Wang SQ, Drda PA. Macromolecules 1996;29:4115–9.
[25] Wang SQ, Drda PA, Inn YW. J Rheol 1996;40(5):875–989.
[26] Barone JR, Plucktaveesak N, Wang SQ. J Rheol 1998;42(4):813–32.
[27] Ui J, Ishimaru Y, Murakami H, Fukushima N, Mori Y. SPE Trans 1964;295–305.
[28] Ballenger TF, Chen I, Crowder JW, Hagler CE, Bogue DC, White JL. Trans Soc Rheol 1971;15:195–215.
[29] Bartos O. J. Appl Phys 1964;35:2767–75.
[30] Baik JJ, Tzoganakis C. Polym Engng Sci 1998;38:274–81.
[31] Fujiyama M, Inata H. J Appl Polym Sci 2002;84:2111–9.
[32] Fujiyama M, Inata H. J Appl Polym Sci 2002;84:2120–7.
[33] Huang JC, Tao Z. J. Appl Polym Sci 2003; in press.
[34] Kazatchkov IB, Hatzikiakos SG, Stewart CW. Polym Engng Sci 1995; 35:1864–71.
[35] Huang JC, Leong KS. J Appl Polym Sci 2002;84:1269–76.
[36] Penwell RC, Porter RS, Middelman S. J Polym Sci, Part A-2 1971;9: 731–45.
[37] Huang JC, Shen HF. Adv Polym Tech 1989;9:211–4.
[38] Huang JC, Liu H, Liu Y. Polym Plast Tech Engng 2001;40:79–88.
[39] Denn MM. Polym Engng Sci 1981;21:65–8.
[40] Binding DM, Couch MA, Walters K. J. Non-Newtonain Fluid Mech 1998;79:137–55.
[41] Christensen JH, Kjaer EM. SPE Technical Paper. 56th ANTEC; 1998. p. 985–9.
[42] Bagley EB. J Appl Phys 1957;28:624–7.
[43] Cogswell FN. Polym Eng Sci 1972;12:64–73.
[44] Ferry JD. Viscoelastic properties of polymers, 3rd ed. New York: Wiley; 1980. Chapter 11.
[45] Piau JM, Kissi NE, Tremblay B. J Non-Newtonian Fluid Mech 1988; 30:197–232.
[46] Brandao J, Spieth E, Lekakou C, Polibrasil SA. Polym Engng Sci 1996;36:49–55.
[47] Tzoganakis C, Vlachopoulos J, Hamielec AE, Shinozaki DM. Polym Engng Sci 1989;29:390–6.
[48] Vlachopoulos J, Alam M. Polym Engng Sci 1972;12:184–92.
[49] Zoller P, Walsh D. Standard pressure–volume–temperature data for polymers. Lancaster, PA: Technomic; 1995. p. 47.
[50] Becker J, Bengtsson P, Klason C, Kubat J, Saha P. Int Polym Proc 1991;6:318–25.
[51] Brochard F, de Gennes PG. Langmuir 1992;8:3033–7.
[52] Okubo S, Hori Y. J Rheol 1980;24(2):253–7.
[53] Akay G. J Non-Newtonian Fluid Mech 1983;13:309–23.